

A Zero-Threshold PT-Symmetric Polariton-Raman Laser

Avijit Dhara^{1†}, Devarshi Chakrabarty^{1†}, Pritam Das^{1†}, Kritika Ghosh², Ayan Roy Chaudhuri², Sajal Dhara^{1*}

¹*Department of Physics, IIT Kharagpur, Kharagpur-721302, India*

²*Materials Science Centre, IIT Kharagpur, Kharagpur-721302, India*

[†] *These authors contributed equally*

^{*} *Corresponding author. email: sajaldhara@phy.iitkgp.ac.in*

Abstract: Parity-time (PT)-symmetry in the classical regime has been realized in optics by introducing loss and gain in electromagnetic wave propagation which has yielded numerous applications like nonreciprocal propagation and finite threshold single-mode lasers. However, PT-symmetry in the quantum regime so far remains elusive. Here, we demonstrate a PT-symmetric zero-threshold polariton-Raman laser by utilizing stimulated resonant Raman scattering of polarized exciton-polaritons. By pumping resonantly at the exceptional point of polariton bands with non-Hermitian topology, a quantum PT-symmetric phase is realized when the Raman-active phonon mode frequencies match with the polariton mode frequency difference. The PT-symmetric phase corresponding to zero-threshold lasing can be switched to PT broken phase showing a finite threshold via cavity detuning by the variation of bath temperature or pump polarization. Our realization of PT-symmetry in the quantum regime and consequently the zero-threshold laser can open up applications in quantum information and stimulate new research activities in cavity quantum electrodynamics.

Microcavity polaritons have proven a promising platform for realizing room temperature superfluidity and highly efficient polariton lasers^{1–3}. Interests have been driven recently in open quantum systems for engineering non-Hermitian topology of polaritonic bands^{4–10}. Hitherto unattained PT-symmetry in such systems in the regime of cavity quantum electrodynamics (CQED) would be indispensable due to its immense potential for applications in photonics, quantum information, and condensed matter physics. The classical PT-symmetric lasers at finite threshold has been achieved so far from the analogy between Schrödinger's equation and the equation of classical electromagnetic wave propagation in a medium^{11–13}. However, theoretically predicted intriguing quantum noise which may lead to inversion-less non-classical lasing mechanism has no analogue in a classical PT-symmetric system^{14–16}. A zero threshold laser can be characterized by high value of coupling factor (β) between spontaneous emission and lasing mode close to unity, which shows up as a linear power dependence in lasing intensity followed by a saturation^{17–22}. Various cavity geometries have been employed to achieve ultralow-threshold Raman lasers in semiconductors^{23–25}, however, a zero threshold laser has never been explored earlier in a Raman system.

In this work, we demonstrate zero threshold polariton Raman laser (ZTPRL) with β value of unity in quantum PT-symmetric phase of a non-Hermitian anisotropic exciton-polariton system. An anisotropic two dimensional (2D) semiconductor has been utilized as the Raman active material embedded in a planar microcavity that supports two non-degenerate cavity modes, along with two highly polarized excitons, resulting in two sets of exciton-polariton bands having near orthogonal polarization states. For a particular polarization of the probe beam, this system enables us to project a specific section of

polariton dispersion in two-dimensional parameter space of polarization and in-plane momentum. Such open quantum systems are being understood recently using non-Hermitian description^{26–35}. The unique property of this system which enables us to achieve the PT-symmetric phase is the existence of phonon mode frequencies matching the frequency difference between one set of polariton modes. This Raman active polaritonic system can thus be pumped to achieve double resonance or stimulated resonant Raman scattering of polaritons with a specific polarization^{36,37}. The PT-symmetric criterion of loss and gain is satisfied between two highly polarized degenerate polaritonic states which are nearly orthogonal as discussed below.

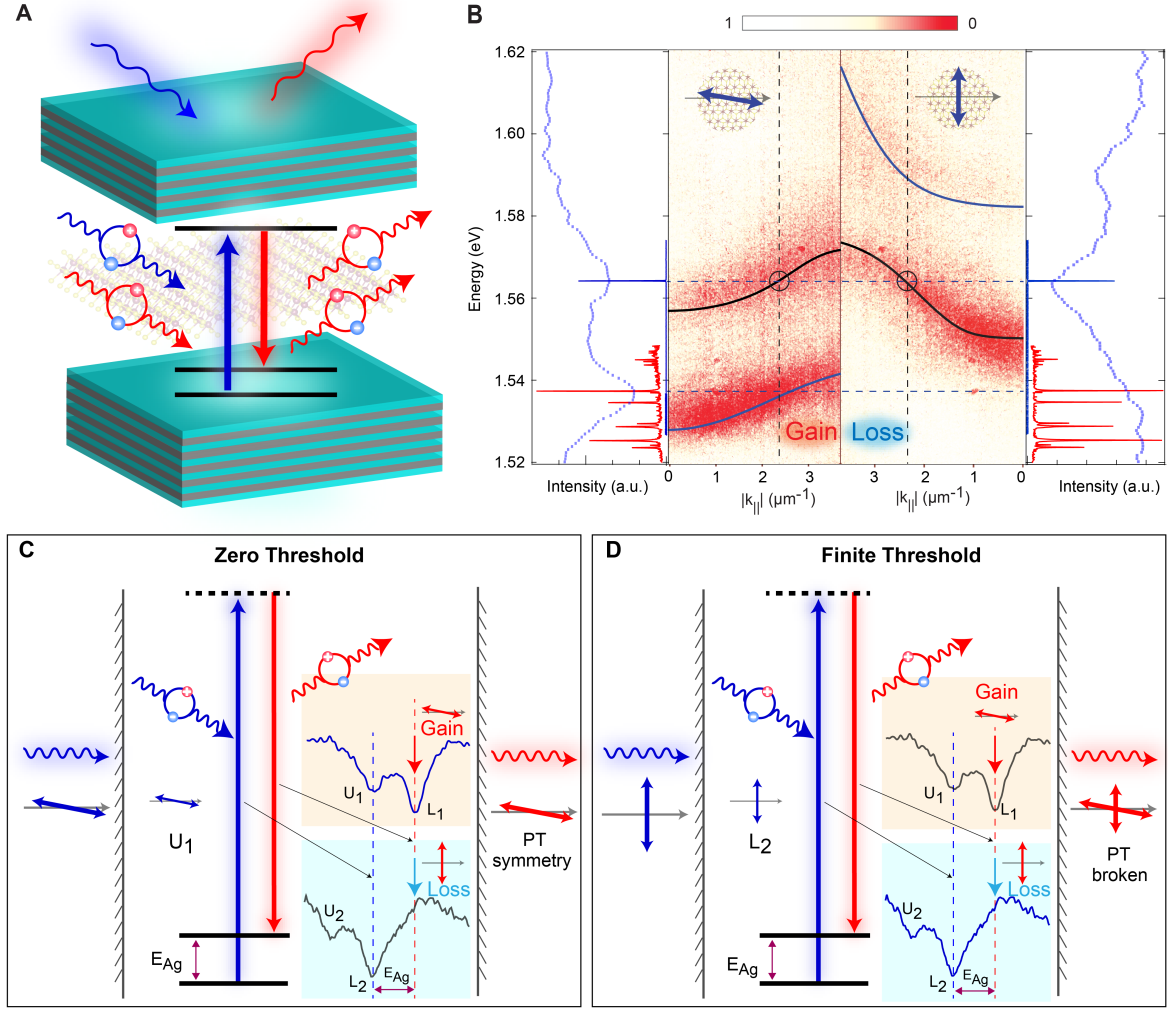


Fig. 1. Schematic and experimental data rendering the mechanism of zero and finite threshold polariton Raman laser. (A) Schematic of a few layer ReS₂ crystal embedded in a $\frac{\lambda}{2}$ optical microcavity, showing stimulated Raman scattering of polaritons. (B) Left (right) panels show angle-resolved reflectance revealing polariton dispersions probed by linearly polarized light along d_1 (d_2) indicated by double sided arrow with respect to crystal b-axis. The EPs at the same energy (~1.564 eV) and momentum in the polariton bands are marked by a black circle. Panels at the extreme left (right) show the Raman spectra overlaid with the reflectance cross-section across the EP obtained from the angle resolved data for pump polarization d_1 (d_2). The pump laser line spectrum is shown near the EP (in blue, intensity in arbitrary scale). (C)-(D) The stimulated resonant Raman mechanism in presence of polaritonic bands polarized along d_1 (C) and d_2 (D). The virtual level of the vibrational state is in resonance with polariton bands as shown in the reflectance line plot (dips at U_1 and L_2). Raman scattering for d_1 polarized excitation undergoes double resonance resulting in single mode zero threshold laser which is d_1 polarized. For d_2 polarized excitation, Raman scattering undergoes single (double) resonance at the EP for d_2 (d_1) polarized polaritons.

Two dimensional semiconductors, are being recognized as a potential active laser medium and an ideal platform for realising exciton-polaritons^{38–43}. A layered transition metal dichalcogenides, ReS₂ is known for its distorted 1T crystal structure hosting strongly polarized excitons, with tunable light-matter coupling^{44–46}. Due to reduced crystal symmetry, ReS₂ has 18 Raman modes in the range of 100 to 450 cm⁻¹⁴⁷. Interestingly we observed presence of dominant Raman peaks and vanishing photoluminescence at near resonance excitation similar to what has been reported recently in ReS₂⁴⁸, which makes it a unique platform to observe the polariton-Raman lasing.

A 10 nm layer of mechanically exfoliated single crystalline ReS₂ is embedded in an optical microcavity (see Materials and Methods in Supporting Information) as shown in the schematic of Fig. 1A. The biaxiality of ReS₂ splits the transverse electric (TE) and transverse magnetic (TM) cavity modes, which interact with two anisotropic excitons (X_1 and X_2) to form four polariton normal modes which we denote as X_1 upper (U_1), X_1 lower (L_1), X_2 upper (U_2) and X_2 lower (L_2) polariton branches. Light-matter interactions in this anisotropic material and the polariton dispersions can be understood by diagonalizing the following Hamiltonian: $H = \hbar\omega_i(k)C_{ik}^\dagger C_{ik} + \hbar\omega_j X_{jk}^\dagger X_{jk} + v_j \hat{e}_i \cdot \hat{d}_j [C_{ik}^\dagger X_{jk} + X_{jk}^\dagger C_{ik}]$. Here, C_{ik} , X_{jk} are the annihilation operators in the in-plane momentum (k) space for the photonic and excitonic modes respectively, \hat{e}_i is the in-plane polarization unit vector of the photonic modes. Indices i and j labels the TE, TM, and two anisotropic excitons X_1 , X_2 respectively. We define the anisotropic axes d_1 and d_2 by observing the absorption maxima with respect to the polarization directions along X_1 and X_2 respectively. These two axes are not exactly orthogonal and make an angle of 170° (d_1) and 90° (d_2) with the crystallographic b-axis respectively, resulting in finite coupling between the X_1 (U_1 , L_1) and X_2 (U_2 , L_2) polariton bands.

Realization of PT-symmetry can be understood from a pair of polaritons corresponding to d_1 and d_2 polarizations undergoing amplification (gain) or dissipation (loss) as shown in the angle resolved reflectivity data in Fig. 1B. These polariton pairs can be pumped selectively, controlled by the polarization of the pump beam. In the left (right) extreme (Fig. 1B) we show the energy of the pump beam, polarized along the d_1 (d_2) axis at the EP and corresponding Stokes lines. For d_1 the Stokes lines coincide within the L_1 band of the cavity polariton mode, and hence undergo amplification. For d_2 the Stokes lines fall in the stop band of the cavity, hence undergoing dissipation. Interestingly, due to non-orthogonality of d_1 and d_2 , both the polariton modes (U_1 and L_2) are being excited at the EP, with amplitudes depending on the pump polarization. The loss and gain mechanism between the polariton pairs originating from the microscopic of Raman scattering is responsible for the intriguing non-Hermitian PT-symmetric phase in the quantum regime. The vibrational energy levels of the lattice and the polaritonic bands as shown in the reflectance plots can be considered separately to understand the double resonance or the stimulated resonant Raman scattering mechanism as shown in Fig. 1C-1D. The mechanism of zero (finite)-threshold laser in the PT-symmetric (PT-symmetric broken) phase when pumped with d_1 (d_2) polarization is shown in Fig. 1C (Fig. 1D).

Several Raman modes are identified from existing literature of ReS₂ with AA stacking order (Method and fig. S1). Out of these Raman peaks we focus on four lines labeled by different colours: A_g^7 (214 cm⁻¹), A_g^{10} (284 cm⁻¹), A_g^{12} (311 cm⁻¹) and A_g^{14} (325 cm⁻¹) as shown in fig 2A and 2C. In Fig. 2A, the stimulated resonant Stokes emission is shown when it was pumped at the EP with energy 1.564 eV (shown in Fig. 1B left panel) and polarization along d_1 . We observed ~150 to 300 times enhancement in the Raman intensity compared to bare ReS₂ of similar thickness on the SiO₂/Si substrate.

The wavelength tunability of Raman lines with pump wavelength is shown in supplementary information fig. S2. As discussed earlier this is the PT-symmetric phase resulting in highly polarized emission lines along d_1 axis as shown in the angular plot at the top inset in Fig. 2A. In this case, the Raman line profile individually overlaps with only one polariton mode (L_1), thus ensuring single mode lasing with $\beta = 1$. Linear power dependence (down to 180 nW, fig. S3) of the Raman intensity reveals the signature of the zero-threshold lasing which gets saturated at higher power as shown in Fig 2B, a trend previously observed in single trapped atom laser from microcavity¹⁸. A rate equation model can be used (see the supplementary materials and methods) to understand this linear power dependence and the saturation behavior which is expected in ZTPRL. The spectral linewidths (~ 0.5 Å) of these Raman peaks are within our spectrometer resolution. Same set of Raman peaks are observed when the pump polarization is switched along d_2 as shown in Fig. 2B. However, striking changes are observed not only in the intensity polar plot, but also in the power dependence as discussed below.

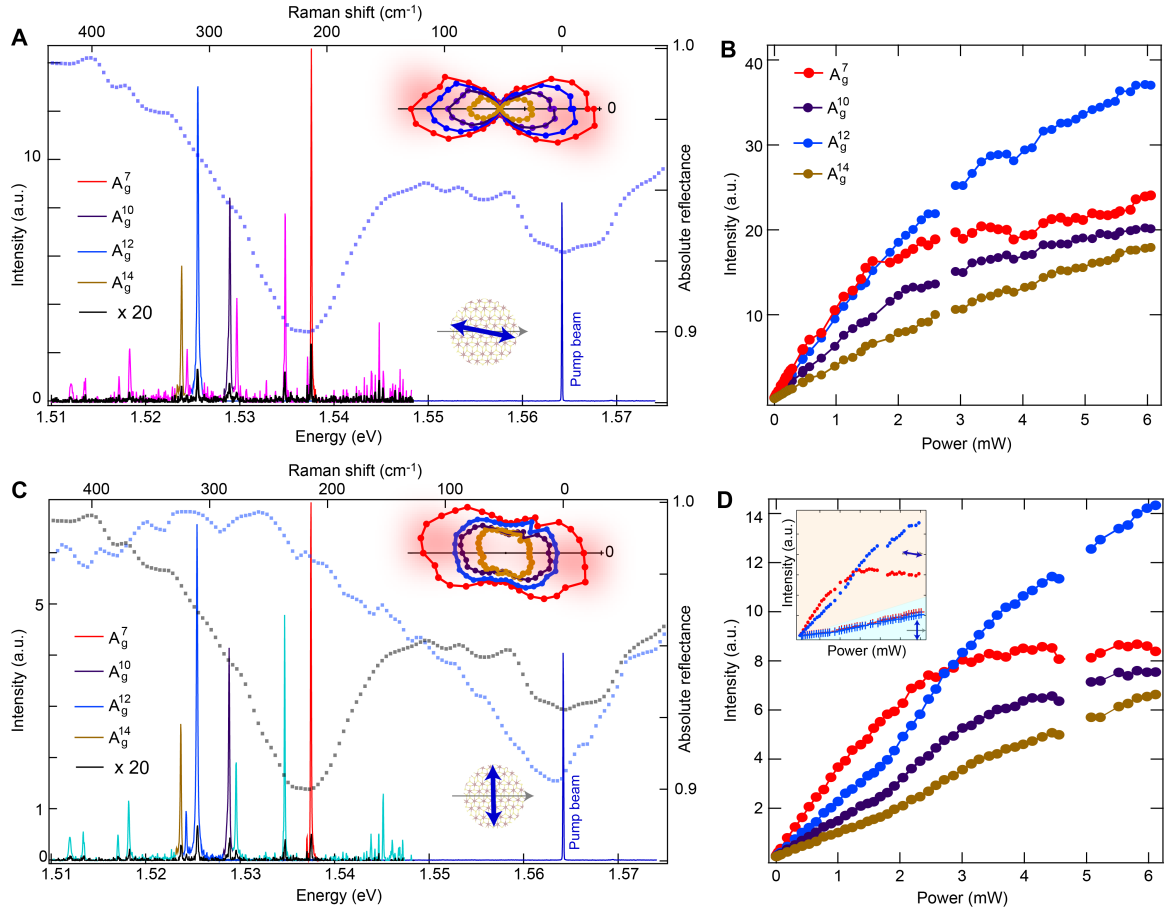


Fig. 2. Polariton Raman laser intensity-power dependence for zero and finite threshold. (A) Raman spectra for d_1 polarized pump with energy 1.564 eV, overlaid with the angle resolved reflectance (dotted line) for d_1 polarized light across the EP (where it is pumped). Four distinct Raman modes are labelled with different colours. The Raman spectra from bare ReS_2 on SiO_2 (black spectrum, multiplied by 20X) is shown in the same plot for comparison. The polarization dependence of four Raman mode intensities with analyzer angle in reference to the b-axis is shown in the inset polar plot. (B) Power dependence of intensity showing zero threshold characteristics for all four Raman modes when the pump polarization is along d_1 . (C) Same as (A) with pump polarization along d_2 , reflectance line plots are overlaid for both d_1 and d_2 polarized polaritons. (D) Same as (B) with pump polarization along d_2 showing the finite threshold lasing behavior with a threshold power around 2 mW for A_g^{10} , A_g^{12} and A_g^{14} . The A_g^7 mode is the most dominant lasing mode having robust zero-threshold characteristics in both the polarizations of the pump beam. The power dependence of the polarization resolved components along d_1 and d_2 are shown in the inset.

Intensity remains maximum along d_1 polarization with a non-zero d_2 component for all the modes as shown in the inset of Fig. 2C. However, a finite threshold of 2 mW is observed with a familiar S-shaped power dependence for the Raman modes A_g^{10} , A_g^{12} and A_g^{14} as shown in Fig. 2D. Polarization resolved power dependence (inset of Fig. 2D.) shows that the lasing action is only happening for the d_1 component, whereas the d_2 component shows a linear power dependence due to spontaneous Raman scattering. This is attributed to the PT-symmetric broken phase as discussed previously in Fig. 1C-1D. However, only one Raman mode (A_g^7), which coincides exactly at the dip of the L_1 band, remains in the PT-symmetric phase and shows ZTPRL irrespective of the pump beam polarization. Thus, the interplay between loss, gain, and the interactions between two differently polarized Stokes polariton modes leading to ZTPRL is controlled by the polarization of the pump beam, where the PT-symmetric system undergoes transition from a PT – symmetric phase (zero-threshold) to a PT – broken phase (finite threshold) as discussed below.

Each point in the polariton band as shown in Fig. 1B represents an energy eigenstate of a polariton mode for a particular in-plane momentum and polarization. We consider two Stokes shifted degenerate states $|\psi_1(\epsilon, k_{EP})\rangle$, and $|\psi_2(\epsilon, k_{EP})\rangle$ vertically below the EP of bands U_1 and L_2 having energies $\epsilon + i\delta_1$, $\epsilon - i\delta_2$ respectively. The sign of the imaginary part in energies are inferred from the observations of gain or loss, where, δ_1 and δ_2 are positive. These states are having finite overlap or coupling (g) due to slight non-orthogonality as discussed earlier. Hamiltonian in this subspace of twofold degenerate states can be written in non-Hermitian form:

$$H = (|\psi_1\rangle, |\psi_2\rangle) \begin{pmatrix} \epsilon + i\delta_1 & g \\ g & \epsilon - i\delta_2 \end{pmatrix} \begin{pmatrix} \langle\psi_1| \\ \langle\psi_2| \end{pmatrix} \dots\dots\dots (1)$$

The eigen values of the above Hamiltonian is given by, $E^\pm = \epsilon + i(\delta_1 - \delta_2)/2 \pm \sqrt{g^2 - \left(\frac{\delta_1 + \delta_2}{2}\right)^2}$.

In the case of finite threshold lasing, we observe one lasing mode and one non-lasing mode at the same energy ($\epsilon = 1.537$ eV). This is only satisfied in the coupling regime, $g < \delta$, where, $\delta = \frac{(\delta_1 + \delta_2)}{2}$, together with the condition, $\delta_1 = \delta_2$ (see the supplementary materials and methods). This is so called the PT-broken phase of a non-Hermitian PT-symmetric Hamiltonian with the diagonal elements being complex conjugate. Our experimental observations suggest that the overlap coupling factor g should depend on the pump polarization, which can be understood as follows: For excitation polarization along d_2 , a large amplitude of $|\psi_2\rangle$ is created, but also attenuated as it falls in the stop band of the cavity. This results in lower interconversion of $|\psi_2\rangle$ to $|\psi_1\rangle$, thus satisfying the condition $g < \delta$, responsible for the finite threshold lasing in PT symmetry broken phase.

On the other hand, ZTPRL is obtained when only a single mode exists inside the cavity, or when the eigenmodes coalesce. This happens in the case when $g \rightarrow \delta = \delta_1 = \delta_2$. In this condition, the eigenvalues are real and degenerate, and the system is in PT-symmetric phase. When excitation is d_1 polarized, a large amplitude of $|\psi_1\rangle$ is created and amplified as it is supported by L_1 , causing enhancement in polarization interconversion of $|\psi_1\rangle$ to $|\psi_2\rangle$. Thus g tends to its maximum $g = \delta$, which is responsible for the zero-threshold lasing action.

From the above discussion, it is expected that if the polariton modes are detuned while keeping the excitation energy fixed, g should change and allow us to observe the zero to finite threshold transition in the power dependence of the emission intensity. This is verified by varying the bath temperature of the system. As temperature increases, a redshift of the polariton modes and an increase in their linewidths changes the reflectance dip in ReS_2 ⁴⁶. This enables us to detune the Stokes polariton modes $|\psi_1\rangle$ and $|\psi_2\rangle$ with respect to the L_1 , and U_2 bands that can influence g and δ .

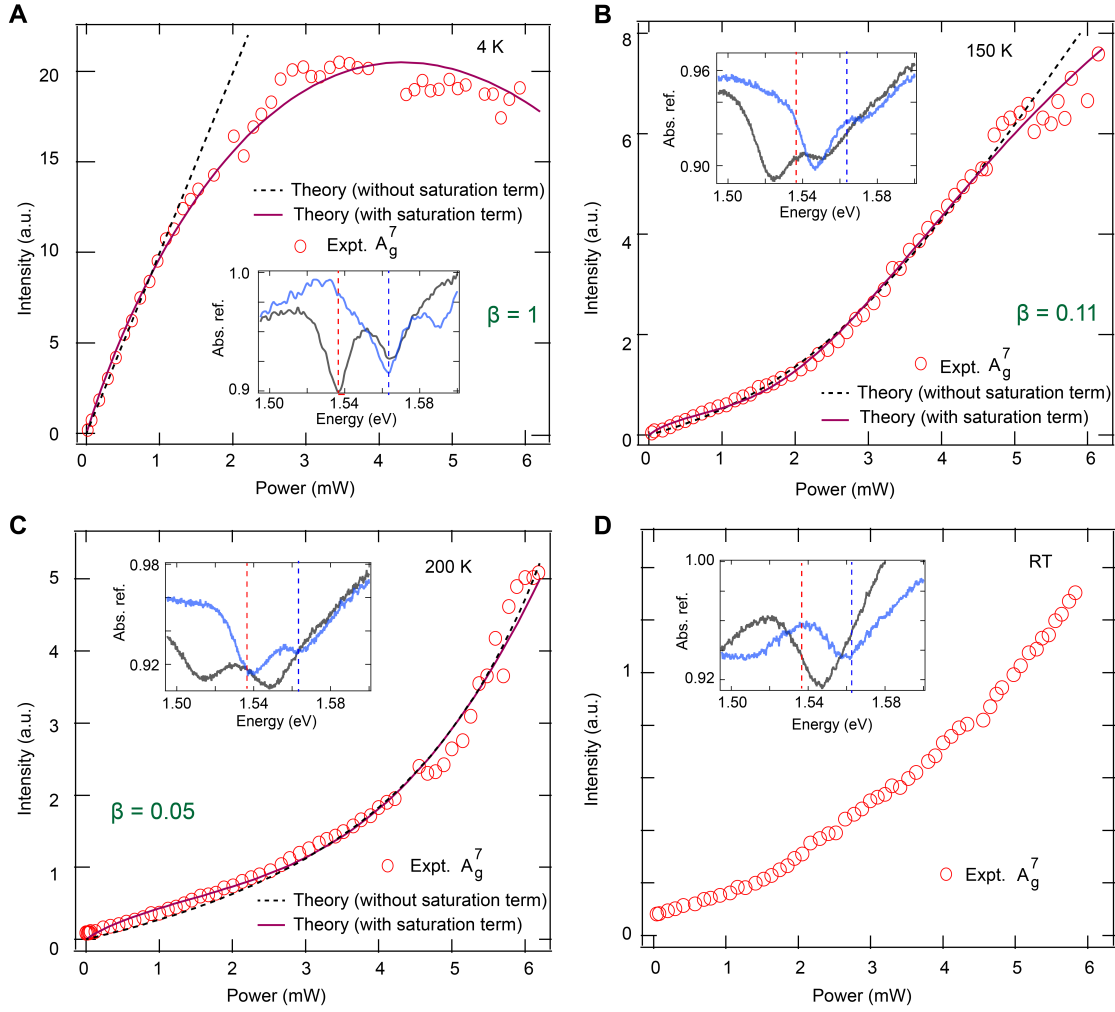


Fig. 3. Zero to finite threshold transition of polariton Raman laser (A_g^7 mode) via cavity detuning and loss at higher temperatures. Power dependence of intensity of the lasing mode when polarization is fixed along d_2 . The circles represent experimental data, solid (dashed) lines are theoretical curves as obtained from the rate equation model with (without) nonlinear saturation as given in the main text (Eq. 2). (A) at 4 K, the power dependence data agrees best with $\beta = 1$. (B) At 150 K, finite threshold is observed with a pre-threshold linear region preceding a kink at 2.3 mW with $\beta = 0.11$. (C) At 200 K, finite threshold persists with a higher threshold pump power of 4.5 mW with $\beta = 0.05$, and (D) At room temperature, lasing threshold is not reached. In each inset, the peak position of A_g^7 mode and the pump energy has been shown (red and blue dashed lines respectively) along with polariton mode absorption dips (grey and red for X_1 and X_2 polariton modes respectively) for different temperatures.

In Fig. 3A-D we show the temperature evolution of the power dependence for the A_g^7 mode which shows robust ZTPRL at 4 K, for polarization of the pump beam along d_2 . At 150 K (Fig. 3B), the polariton branch is redshifted with a broader linewidth (shown in the inset of fig 3B). A prominent non-linear power dependence is observed with a finite threshold power of 2.3 mW, as shown in Fig. 3B, indicating transition from zero to finite threshold due to change in g and δ . Further reduction in g and increment in δ via detuning and loss is observed at 200 K, resulting in a threshold power of 4.5 mW. Polariton modes are almost absent at room temperature as shown in Fig. 3D, except the non-degenerate cavity modes whose separation is greater than the phonon energies and hence the system cannot reach the threshold condition within the range of power variation. Since the rate equation model applies only for double resonance condition, we do not use it for fitting in this case.

Each Raman mode within the polariton bands give rise to single mode lasing, therefore, to understand the power dependence in this system we use a rate equation model for the doubly resonant Raman scattering by treating individual Raman modes separately. We relate the Stokes polaritons intensity (I_{out}) with the polariton pump power (P_{int}) as follows (see the supplementary materials and methods):

$$I_{out} \propto \frac{1}{2} \left(P_{int} + \beta - 1 - \beta F - G + \sqrt{(\beta - 1 - P_{int} + \beta F + G)^2 + 4\beta F P_{int}} \right) \dots\dots\dots (2)$$

Where the spontaneous emission coupling factor $\beta \leq 1$, the equality holds when a single photonic mode is present in the cavity, which happens only in the PT-symmetric phase. In case of zero threshold lasing (in the PT-symmetric condition) where $\beta = 1$, the power dependence is linear as shown using dashed lines in Fig.3A and Fig. 4A. The observed saturation at higher power can be attributed to 3rd order non-linear processes whose effect can be captured by including a saturation term ($\propto P_{int}^{3/2}$) in the above relation, as shown by the solid lines in Fig. 3A-C and 4. For more than one mode ($\beta < 1$), I_{out} vs P_{int} is a nonlinear S-shaped curve, which is characteristic of finite threshold lasing.

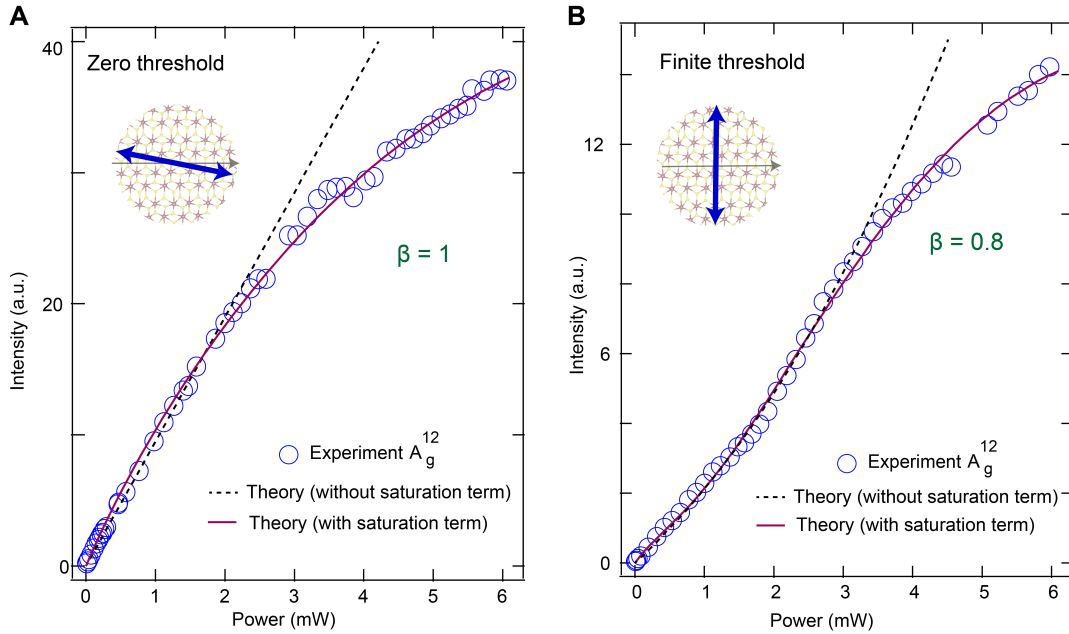


Fig. 4. Zero to finite threshold transition of polariton Raman laser via polarization of pump beam. Power dependence of the A_g^{12} lasing mode at two different pump polarizations. The empty circles represent experimental data, solid (dashed) lines are theoretical curves as obtained from the rate equation model with (without) nonlinear saturation as given in the main text (Eq. 2). **(A)** Pump polarization along d_1 when the power dependence data agrees best with $\beta = 1$. **(B)** Pump polarization is switched along d_2 with the power dependence data showing finite threshold power of 1.9 mW which agrees well with $\beta = 0.8$.

Switching between the PT-symmetric ($\beta = 1$) to PT-broken phase ($\beta < 1$), controlled by the polarization of the pump beam, shows up with distinct power dependence of A_g^{12} mode that can be modeled with $\beta = 1$ for d_1 polarized excitation which changes to $\beta = 0.8$ for d_2 polarized excitation as shown in Fig. 4A. The variation of β as a function of temperature giving rise to the transition between ZTPRL to finite threshold lasing as discussed above, can be observed in Fig. 3A-C at three different temperatures. Here β varies from unity at 4 K to 0.05 at 200 K.

All the lasing modes that have been discussed are directional, with different angles of emission satisfying momentum matching conditions as shown in the angle resolved measurement in the Fig. S6. However, no directionality has been observed for any of the non-lasing modes irrespective of

enhancement of Raman intensities. The robustness of zero threshold lasing and all the experimental results as discussed above has been observed in a different ReS₂ flake of similar thickness inside the same cavity, rotated and brought to the same orientation as the previous one, which is shown in the fig S8. Note that the polariton dispersions, occurrence of EP, and the realization of PT-symmetry as presented in Fig. 1B, depends on the angular orientation of the sample which has been discussed in detail in our recent work ⁶. A different orientation of the same sample thus allows us to excite the system at the same energy of the pump beam where there is no EP as shown in the Fig. S7. In this orientation which we obtain by rotating the sample by 45 degree, a robust ZTPRL has been observed for all four Raman modes when the pump polarization is along d_1 , however, the power dependence becomes linear and therefore, no lasing is observed for d_2 polarized pump. In addition, the intensity polar plot becomes very different as shown in the Supplementary Fig. S8. Therefore, in the absence of EP, ZTPRL or PT-symmetric phase can be observed only for the d_1 polarized excitation, however, it cannot be transformed to a PT broken phase at a different pump polarization of d_2 .

Conclusion and outlook

In conclusion, we demonstrated zero threshold PT-symmetric polariton Raman laser in a system of anisotropic microcavity exciton-polaritons. To the best of our knowledge this work highlights for the first time the significance of PT symmetry in an open quantum system of exciton-polaritons for the realization of zero threshold lasers in a solid-state system. This work demonstrates that non-degenerate cavity modes due to microscopic anisotropy of the Raman active medium is an essential ingredient to achieve the PT-symmetry ensuring the β factor value of unity for the single mode lasing. The shift from PT symmetry phase to PT broken phase is clearly visualized by bringing the system from zero to finite threshold regime. We expect that the thresholdless lasing action demonstrated in our system is quite generic and could be observed in any single mode microcavity hosting anisotropic Raman active materials supporting polarized excitons. We believe our work not only paves the way to a new frontier in quantum science and technology involving non-Hermitian PT-symmetry and topological polaritons, but also offers a significant advance in the realm of tunable, thresholdless microlasers with numerous applications in quantum optics and information.

Acknowledgements:

This work has been supported by funding from the Science and Engineering Research Board (CRG/2018/002845, CRG/2021/000811); Ministry of Education (MoE/STARS- 1/647); Council of Scientific and Industrial Research, India (09/081(1352)/2019-EMR-I); Department of Science and Technology, Ministry of Science and Technology, India (IF180046) and Indian Institute of Technology Kharagpur. We thank Prof. Sugata Pratik Khastgir for valuable discussions with him during this work.

Author contributions:

SD conceptualized the project. AD, DC, KG, ARC and SD contributed in the sample fabrication. AD, DC, PD and SD formulated the experiments, performed data analysis, and developed the theory. AD, DC, PD performed all optical measurements. AD, DC, PD and SD drafted the paper, and all authors contributed to reviewing and editing the final draft. SD supervised the project.

References:

1. Amo, A. *et al.* Superfluidity of polaritons in semiconductor microcavities. *Nature Phys* **5**, 805–810 (2009).
2. Christopoulos, S. *et al.* Room-Temperature Polariton Lasing in Semiconductor Microcavities. *Phys. Rev. Lett.* **98**, 126405 (2007).
3. Balili, R., Hartwell, V., Snoke, D., Pfeiffer, L. & West, K. Bose-Einstein Condensation of Microcavity Polaritons in a Trap. *Science* **316**, 1007–1010 (2007).
4. Gao, W., Li, X., Bamba, M. & Kono, J. Continuous transition between weak and ultrastrong coupling through exceptional points in carbon nanotube microcavity exciton–polaritons. *Nature Photonics* **12**, 362–367 (2018).
5. Gao, T. *et al.* Observation of non-Hermitian degeneracies in a chaotic exciton-polariton billiard. *Nature* **526**, 554–558 (2015).
6. Chakrabarty, D., Dhara, A., Das, P., Ghosh, K. & Chaudhuri, A. R. Anisotropic exciton polariton pairs as a platform for PT- symmetric non-Hermitian physics. 10.48550/arXiv.2305.17472
7. Yuen-Zhou, J. *et al.* Plexciton Dirac points and topological modes. *Nat Commun* **7**, 11783 (2016).
8. Song, H. G., Choi, M., Woo, K. Y., Park, C. H. & Cho, Y.-H. Room-temperature polaritonic non-Hermitian system with single microcavity. *Nat. Photon.* **15**, 582–587 (2021).
9. Su, R. *et al.* Direct measurement of a non-Hermitian topological invariant in a hybrid light-matter system. *Science Advances* **7**, eabj8905 (2021).
10. Bergholtz, E. J., Budich, J. C. & Kunst, F. K. Exceptional topology of non-Hermitian systems. *Rev. Mod. Phys.* **93**, 015005 (2021).
11. Feng, L., Wong, Z. J., Ma, R.-M., Wang, Y. & Zhang, X. Single-mode laser by parity-time symmetry breaking. *Science* **346**, 972–975 (2014).
12. Hodaei, H., Miri, M.-A., Heinrich, M., Christodoulides, D. N. & Khajavikhan, M. Parity-time–symmetric microring lasers. *Science* **346**, 975–978 (2014).

13. Feng, L., El-Ganainy, R. & Ge, L. Non-Hermitian photonics based on parity–time symmetry. *Nature Photon* **11**, 752–762 (2017).
14. Kepesidis, K. V. *et al.* -symmetry breaking in the steady state of microscopic gain–loss systems. *New J. Phys.* **18**, 095003 (2016).
15. Zhang, L., Agarwal, G. S., Schleich, W. P. & Scully, M. O. Hidden \mathcal{PT} symmetry and quantization of a coupled-oscillator model of quantum amplification by superradiant emission of radiation. *Phys. Rev. A* **96**, 013827 (2017).
16. El-Ganainy, R. *et al.* Non-Hermitian physics and PT symmetry. *Nature Phys* **14**, 11–19 (2018).
17. Yamamoto, Y. & Slusher, R. E. Optical Processes in Microcavities. *Physics Today* **46**, 66–73 (1993).
18. McKeever, J., Boca, A., Boozer, A. D., Buck, J. R. & Kimble, H. J. Experimental realization of a one-atom laser in the regime of strong coupling. *Nature* **425**, 268–271 (2003).
19. Khajavikhan, M. *et al.* Thresholdless nanoscale coaxial lasers. *Nature* **482**, 204–207 (2012).
20. Prieto, I. *et al.* Near thresholdless laser operation at room temperature. *Optica, OPTICA* **2**, 66–69 (2015).
21. Wu, K., Park, Y.-S., Lim, J. & Klimov, V. I. Towards zero-threshold optical gain using charged semiconductor quantum dots. *Nature Nanotech* **12**, 1140–1147 (2017).
22. Jagsch, S. T. *et al.* A quantum optical study of thresholdless lasing features in high- β nitride nanobeam cavities. *Nat Commun* **9**, 564 (2018).
23. Spillane, S. M., Kippenberg, T. J. & Vahala, K. J. Ultralow-threshold Raman laser using a spherical dielectric microcavity. *Nature* **415**, 621–623 (2002).
24. Grudinin, I. S. & Maleki, L. Ultralow-threshold Raman lasing with CaF_2 resonators. *Opt. Lett., OL* **32**, 166–168 (2007).
25. Takahashi, Y. *et al.* A micrometre-scale Raman silicon laser with a microwatt threshold. *Nature* **498**, 470–474 (2013).
26. Rüter, C. E. *et al.* Observation of parity–time symmetry in optics. *Nature Phys* **6**, 192–195 (2010).

27. Peng, B. *et al.* Parity–time-symmetric whispering-gallery microcavities. *Nature Phys* **10**, 394–398 (2014).
28. Chang, L. *et al.* Parity–time symmetry and variable optical isolation in active–passive-coupled microresonators. *Nature Photon* **8**, 524–529 (2014).
29. Richter, S. *et al.* Exceptional points in anisotropic planar microcavities. *Phys. Rev. A* **95**, 023836 (2017).
30. Gao, T. *et al.* Chiral Modes at Exceptional Points in Exciton-Polariton Quantum Fluids. *Phys. Rev. Lett.* **120**, 065301 (2018).
31. Zhang, J. *et al.* A phonon laser operating at an exceptional point. *Nature Photon* **12**, 479–484 (2018).
32. Kremer, M. *et al.* Demonstration of a two-dimensional \mathcal{PT} -symmetric crystal. *Nat Commun* **10**, 435 (2019).
33. Miri, M.-A. & Alù, A. Exceptional points in optics and photonics. *Science* **363**, eaar7709 (2019).
34. Özdemir, Ş. K., Rotter, S., Nori, F. & Yang, L. Parity–time symmetry and exceptional points in photonics. *Nat. Mater.* **18**, 783–798 (2019).
35. Khurgin, J. B. Exceptional points in polaritonic cavities and subthreshold Fabry–Perot lasers. *Optica, OPTICA* **7**, 1015–1023 (2020).
36. Fainstein, A., Jusserand, B. & Thierry-Mieg, V. Raman Scattering Enhancement by Optical Confinement in a Semiconductor Planar Microcavity. *Phys. Rev. Lett.* **75**, 3764–3767 (1995).
37. Fainstein, A., Jusserand, B. & Thierry-Mieg, V. Cavity-Polariton Mediated Resonant Raman Scattering. *Phys. Rev. Lett.* **78**, 1576–1579 (1997).
38. Wang, G. *et al.* *Colloquium* : Excitons in atomically thin transition metal dichalcogenides. *Rev. Mod. Phys.* **90**, 021001 (2018).
39. Wu, S. *et al.* Monolayer semiconductor nanocavity lasers with ultralow thresholds. *Nature* **520**, 69–72 (2015).
40. Ye, Y. *et al.* Monolayer excitonic laser. *Nature Photon* **9**, 733–737 (2015).

41. Shang, J. *et al.* Room-temperature 2D semiconductor activated vertical-cavity surface-emitting lasers. *Nat Commun* **8**, 543 (2017).
42. Liu, X. *et al.* Strong light–matter coupling in two-dimensional atomic crystals. *Nature Photon* **9**, 30–34 (2015).
43. Dhara, S. *et al.* Anomalous dispersion of microcavity trion-polaritons. *Nature Phys* **14**, 130–133 (2018).
44. Aslan, O. B., Chenet, D. A., van der Zande, A. M., Hone, J. C. & Heinz, T. F. Linearly Polarized Excitons in Single- and Few-Layer ReS₂ Crystals. *ACS Photonics* **3**, 96–101 (2016).
45. Dhara, A. *et al.* Additional excitonic features and momentum-dark states in ReS₂. *Phys. Rev. B* **102**, 161404 (2020).
46. Chakrabarty, D. *et al.* Interfacial anisotropic exciton-polariton manifolds in ReS₂. *Optica, OPTICA* **8**, 1488–1494 (2021).
47. McCreary, A. *et al.* Intricate Resonant Raman Response in Anisotropic ReS₂. *Nano Lett.* **17**, 5897–5907 (2017).
48. Jadczyk, J. *et al.* Exciton binding energy and hydrogenic Rydberg series in layered ReS₂. *Sci Rep* **9**, 1578 (2019).

Supplementary Materials for
A Zero-Threshold PT-Symmetric Polariton-Raman Laser

Avijit Dhara^{1†}, Devarshi Chakrabarty^{1†}, Pritam Das^{1†}, Kritika Ghosh², Ayan Roy Chaudhuri², Sajal Dhara^{1*}

¹*Department of Physics, IIT Kharagpur, Kharagpur-721302, India*

²*Materials Science Centre, IIT Kharagpur, Kharagpur-721302, India*

[†] *These authors contributed equally*

^{*} *Corresponding author. email: sajaldhara@phy.iitkgp.ac.in*

The file includes:

Materials and Methods

Figs. S1 to S9

Table S1 and S2

References

Materials and Methods

Sample fabrication

We prepared three samples of ReS_2 with the same thickness: two embedded in a microcavity and the other stacked on SiO_2/Si (henceforth also referred to as a 'bare' sample). The microcavity consists of two distributed Bragg reflectors (DBRs). The bottom mirror comprises 10 pairs of $\text{SiO}_2/\text{Ta}_2\text{O}_5$ films, grown using the RF sputtering technique. Two ReS_2 crystal of thickness 10 nm are exfoliated by the dry transfer method and transferred on the bottom mirror. The top DBR of 8 pairs of $\text{SiO}_2/\text{Ta}_2\text{O}_5$ is then deposited using the same sputtering method. The other sample is prepared by dry transfer of exfoliated 10 nm thick ReS_2 crystal on the Si/SiO_2 substrate. We estimate the sample thickness from optical contrast. Sample image is shown in the fig. S4.

Measurement

All optical measurements were performed with the sample placed in a closed cycle microscopy cryostat (Montana Instruments) with a variable temperature range of 3.2 to 295 K. For the Raman study, we excite the sample using backscattering geometry with a Ti: Sapphire laser (Coherent—MIRA) in CW mode with a pump energy of 1.564 eV ($\lambda_{\text{excitation}} = 792.8 \text{ nm}$). The excitation path contains a linear polarizer followed by a half-wave plate mounted on a motorized rotational stage to control the polarization of the pump beam. Polarization state of light beam was preserved throughout the optical path via a special design in our optical setup as discussed elsewhere¹ for polarization resolved Raman spectroscopy. The laser beam was focused to a spot size $\sim 1 \mu\text{m}$ by a 60X objective lens with numerical aperture of 0.7. The Raman stokes signal is collected through the same objective lens and dispersed by a diffraction grating with 1200 grooves per mm and detected by a nitrogen-cooled CCD (Pylon 400) with spectral resolution of 0.5 cm^{-1} . In the temperature dependent power variation study, to attenuate scattered light of the laser from the optical elements in the beam path and increase the signal-to-noise ratio, an analyzer is kept before the spectrometer, crossed with the laser polarization. A broadband light source (Thorlabs SLS202L) is used for reflectance measurements.

Stacking order in ReS_2

We identify several Raman modes which exactly match with existing literature^{2,3}, such as: A_g^4 (139 cm^{-1}), A_g^5 (144 cm^{-1}), A_g^1 (152 cm^{-1}), A_g^7 (214 cm^{-1}), A_g^8 (236 cm^{-1}), A_g^9 (276 cm^{-1}), A_g^{10} (284 cm^{-1}), A_g^{12} (311 cm^{-1}), A_g^{13} (320 cm^{-1}), A_g^{14} (325 cm^{-1}), A_g^{15} (349 cm^{-1}), A_g^{16} (369 cm^{-1}), A_g^{17} (378 cm^{-1}), A_g^{18} (408 cm^{-1}), A_g^3 (420 cm^{-1}) and A_g^2 (440 cm^{-1}), shown in fig. S5.

Recently, it has been reported that ReS_2 crystal has two stable stacking orders (AA and AB)³, which have been identified by the separation between the A_g^4 and A_g^1 modes. The separation between these two modes in both cases (inside microcavity and bare sample) is 13 cm^{-1} , as found in AA stacking ReS_2 crystal, as shown in fig. S1.

Model for Non-Hermitian PT-Symmetric system

The eigenvalues of the matrix from Eqn. (1) are:

$$E^{\pm} = \epsilon + i(\delta_1 - \delta_2)/2 \pm \sqrt{g^2 - \left(\frac{\delta_1 + \delta_2}{2}\right)^2} \dots\dots\dots (3)$$

In the case of finite threshold lasing (pumping along d_2 polarization), we observe one lasing mode (polarized along d_1) and one non-lasing mode (polarized along d_2) at the same energy (ϵ). Thus, the two eigenvalues E^{\pm} must satisfy the following conditions: (i) real part should be the same (ϵ), and (ii) imaginary part should be opposite in sign, positive sign implying lasing mode and negative sign lossy mode. Condition (i) is satisfied in the regime, $g \leq \delta$, where $\delta = \frac{(\delta_1 + \delta_2)}{2}$. Since the quantity $\sqrt{g^2 - \left(\frac{\delta_1 + \delta_2}{2}\right)^2}$ is always smaller than $\frac{(\delta_1 - \delta_2)}{2}$, condition (ii) is only possible when $\frac{(\delta_1 - \delta_2)}{2} = 0$, which implies $\delta_1 = \delta_2$. Thus, from our arguments, based on pure experimental observations, we find the Hamiltonian H is PT-symmetric, since the diagonal elements are complex conjugates:

$$H = \begin{pmatrix} \epsilon + i\delta & g \\ g & \epsilon - i\delta \end{pmatrix}$$

The mode E^+ with a positive imaginary part is responsible for finite threshold mode, and E^- non-lasing lossy mode of the cavity. For excitation polarization along d_2 , a large amplitude of $|\psi_2\rangle$ lies in the stop band of the cavity, leading to a weak coupling ($g < \delta$) condition and hence finite threshold lasing in PT broken phase.

On the other hand, ZTPRL is obtained when only a single mode exists inside the cavity, or the eigenmodes coalesce. This happens in the case when $g = \delta$. In this condition, the eigenvalues are real and degenerate, and the system is in PT-symmetric phase. Our experimental observations suggest that the coupling strength g should depend on the pump polarization, which can be understood as follows: When excited along d_1 polarization, a large amplitude of $|\psi_1\rangle$ being amplified as it is supported by L_1 causing the enhancement in g reaches its maximum $g = \delta$, showing zero-threshold lasing. Interestingly, we observe only the A_g^7 mode which coincides exactly at the dip of the L_1 band shows ZTPRL irrespective of the polarization of the pump beam.

Rate equation model for zero and finite threshold PT- symmetric polariton Raman laser

The power dependent intensity of polariton Raman laser in the zero and finite threshold regime can be understood from the rate equation model for stimulated resonant Raman scattering⁴⁻⁹ we describe below (schematic shown in fig. S9).

Polaritons are pumped in state $|\psi(\epsilon_{EP}, k_{EP})\rangle$ at the EP of bands U_1 and L_2 , with rate $P_{int} = c_1 P_i$, where P_i is the external pump power of the laser incident on the sample. Through free-space spontaneous Raman scattering (with rate S), the pumped polaritons are instantaneously scattered into the degenerate ground states $|\psi_1(\epsilon, k_{EP})\rangle$, $|\psi_2(\epsilon, k_{EP})\rangle$, having the same momentum but different polarizations. Stokes polariton modes are thus emitted along d_1 and d_2 polarizations. The Stokes polariton modes along d_1 polarization is confined in the cavity via the L_1 polariton branch, which stimulate the Raman scattering rate (S) by the Purcell factor (F), creating the lasing mode with energy E^+ . On the other hand, Stokes polariton modes along d_2 direction fall in the stopband and are not confined, forming the lossy mode with energy E^- . The spontaneous emission rate from lasing and lossy mode is βSF and $(1 - \beta)S$ respectively. Additionally, stimulated scattering rate of the

pumped polaritons is βSFN_S , where N_S is the number of photons associated with Stokes polariton mode in the cavity, with a decay rate γ_c . GS signifies the radiative and non-radiative loss rate of the pumped polaritons.

The rate equations can be written as,

$$\frac{dN_P}{dt} = - (1 - \beta)SN_P - (\beta SFN_P + \beta SFN_S N_P) - GS N_P + P_{int} \quad \text{..... (4)}$$

$$\frac{dN_S}{dt} = (\beta SFN_P + \beta SFN_S N_P) - \gamma_c N_S \quad \text{..... (5)}$$

Here, N_P is the occupancy of pumped polaritons.

The solution of the equation (4) and (5) can be written as,

$$I_{out} = c' N_S \gamma_c = \frac{1}{2} c_2 \left(c_1 P_i + \beta - 1 - \beta F - G + \sqrt{(1 - \beta - c_1 P_i + \beta F + G)^2 + 4\beta F c_1 P_i} \right) \quad \text{.....(6)}$$

The parameter c_1 is the conversion factor relating the actual pump polariton population inside the cavity to the external actual power (P_i). c_1 varies with the polariton absorption linewidth which can be captured in the temperature dependence (given in Table S1 & S2). Parameter $c_2 = c' \gamma_c$ is the conversion ratio of the actual Stokes polariton decay rate ($c' N_S \gamma_c$) from the cavity and the intensity count (I_{out}) in the spectrometer CCD. Parameter c_2 also varies with temperature due to detuning and linewidth variation of polaritons as temperature is varied (shown in Table S1&S2).

To capture the saturation behavior at higher power we add a 3rd order nonlinear term $c_3 P_i^{1.5}$ in equation (6) by introducing a proportionality parameter c_3 :

$$I_{out} = \frac{1}{2} c_2 \left(c_1 P_i + \beta - 1 - \beta F - G + \sqrt{(\beta - 1 - c_1 P_{int} + \beta F + G)^2 + 4\beta F c_1 P_i} \right) - c_3 P_i^{1.5} \quad \text{.....(7)}$$

To fit the measured intensity shown in Fig 4 which includes both the lasing and lossy component, we also account for the occupancy of the lossy polarization mode:

$$\frac{dN_L}{dt} = (1 - \beta)SN_P - \gamma_L N_L \quad \text{.....(8)}$$

This yields the total intensity from both the lasing and lossy modes:

$$I_{out,unpol} = I_{out} + \frac{c_2(1-\beta)I_{out}}{c_2\beta F + I_{out}} \quad \text{..... (9)}$$

All the fitted parameters are listed in the Table S1 and S2.

Table S1. Parameters obtained from fitting power dependence of A_g^{12} mode at 4K for d_1 and d_2 excitation polarization (Fig 4)

Table S1A. Without saturation term

	F from fitting	β	c_1	c_2	G
Excitation polarization along d_1	39	1	50	187	0
Excitation polarization along d_2	40	0.8	28	510	206

Table S1B. With saturation term

	F from fitting	β	c_1	c_2	c_3	G
Excitation polarization along d_1	35	1	56	236	2900	0
Excitation polarization along d_2	40	0.8	56	190	2613	72

Table S2. Parameters obtained from fitting power dependence of A_g^7 mode at different temperatures for fixed excitation polarization d_2 (Fig 3)

Table S2A. Without saturation term

Temperature	F from fitting	β	G	c_1	c_2
4 K	80	1	0	54	185
150 K	39	0.11	75	14	550
200 K	20	0.05	20	3	2042

Table S2B. With saturation term

Temperature	F from fitting	β	G	c_1	c_2	c_3
4 K	77	1	0	144	38	4560
150 K	40	0.11	16	8	841	1359
200 K	25	0.05	9	1.5	4759	465

Note: All the values of Purcell factor (F) and β obtained from fitting in Tables S1 and S2 agree well with our theoretically calculated values.

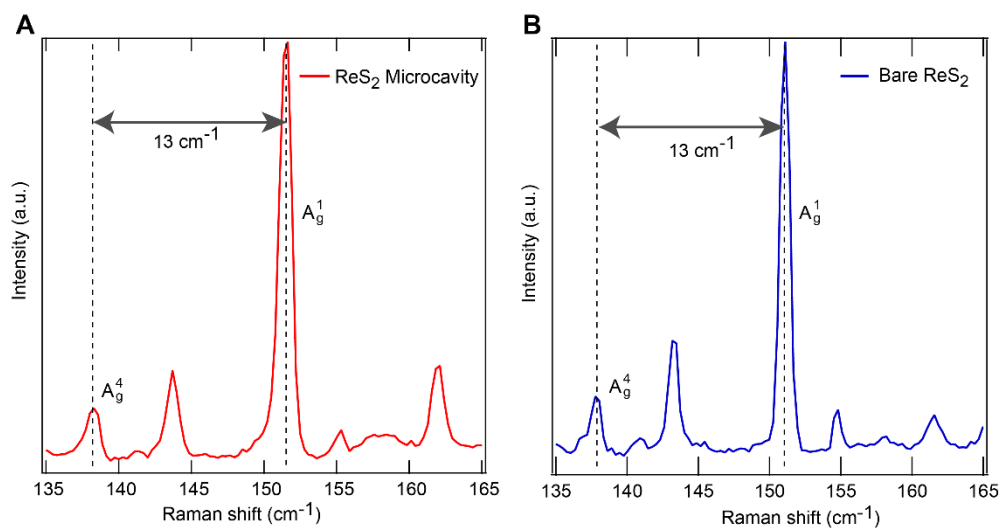


Fig. S1. Stacking order dependent Raman modes in ReS₂. The A_g^4 and A_g^1 Raman modes exhibit a separation of 13 cm^{-1} indicating AA stacking in both scenarios: (A) ReS₂ within the microcavity and (B) ReS₂ on SiO₂/Si

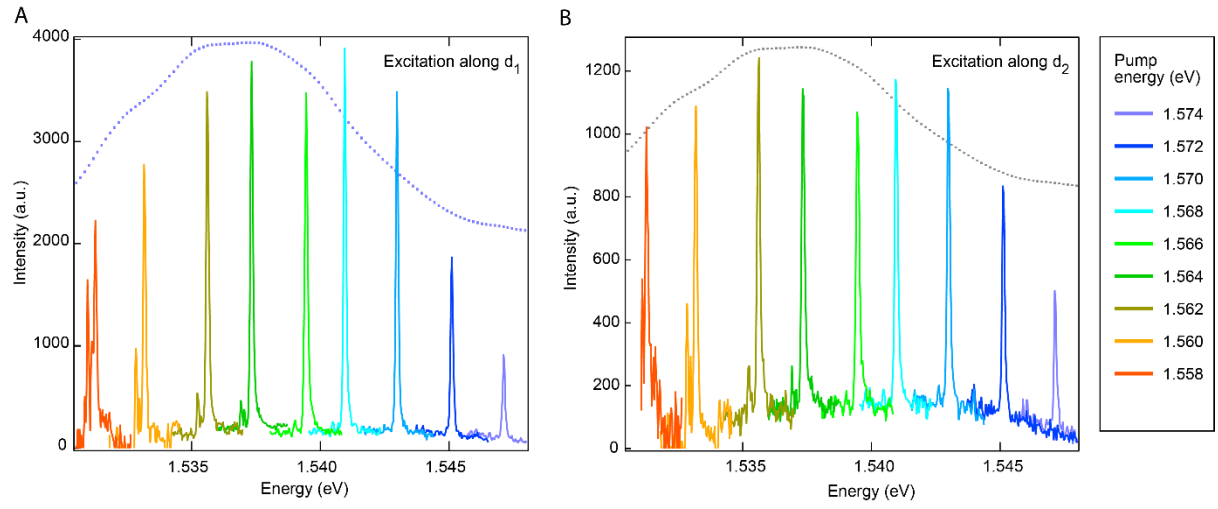


Fig. S2. Intensity variation of A7g as a function of pump energy. (A) For d_1 excitation, the intensity of the A7g mode (represented with different colors for different excitation energy) becomes maximum when it coincides with the minima of the reflectance dip of L_1 . (B) For excitation along d_2 , a similar intensity variation pattern has been observed following the L_1 polariton branch instead of L_2 . The absolute reflectance dip from Fig 2A has been inverted as a visual aid with blue and black dots in the background in both figures.

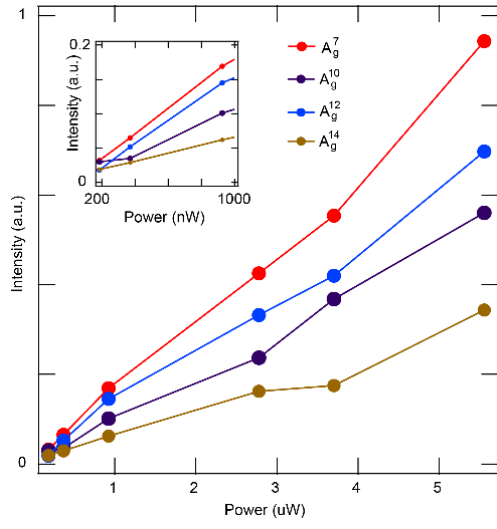


Fig. S3. Threshold scan in hundreds of nW range for the case of zero threshold lasing when pump beam polarization is along d_1 .

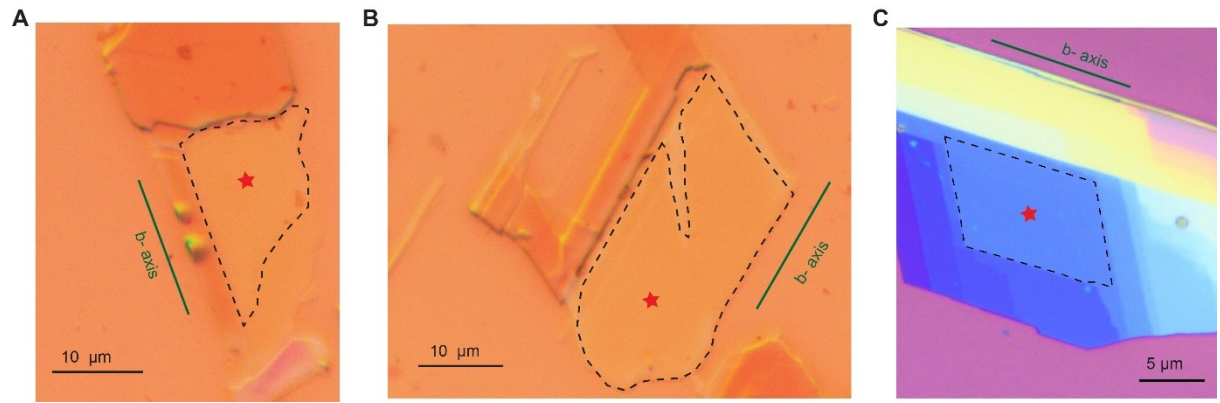


Fig. S4. Optical microscope images of (A) ReS₂ inside microcavity. All data presented in Figs. 1-4 in the article correspond to experiments done on this sample. **(B)** Different ReS₂ sample inside microcavity with same thickness as (A) whose corresponding experimental data is shown in fig S8. **(C)** Bare ReS₂ (ReS₂ on SiO₂/Si). The black dotted lines indicate the boundary of the sample section that is 10 nm in thickness. The red starting point denotes the excitation point.

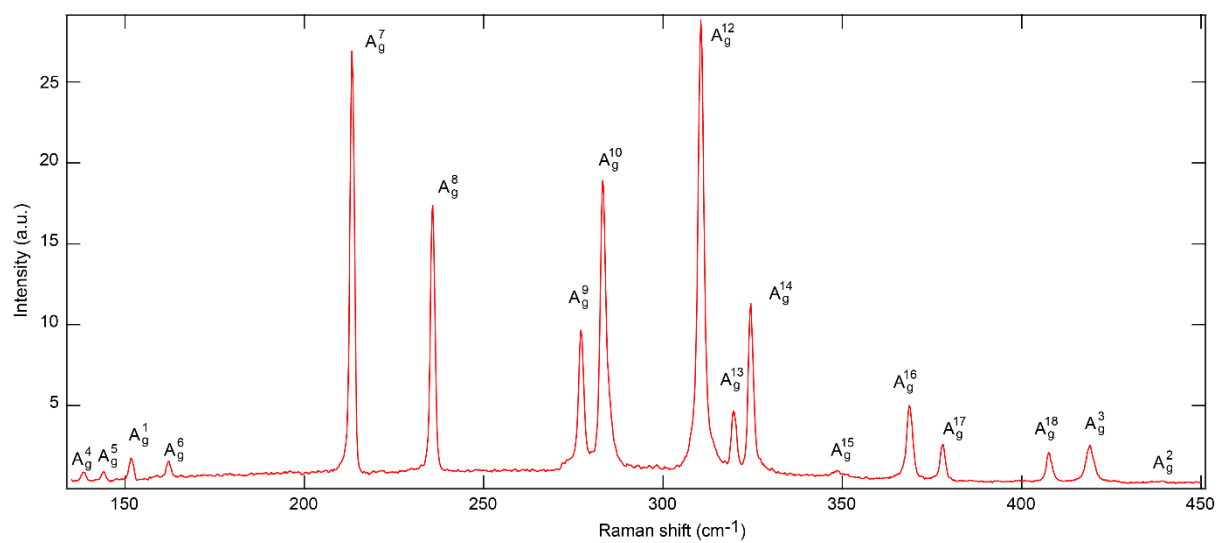


Fig. S5. Stokes Raman spectra measured for ReS₂ inside microcavity, with the distinct modes labelled.

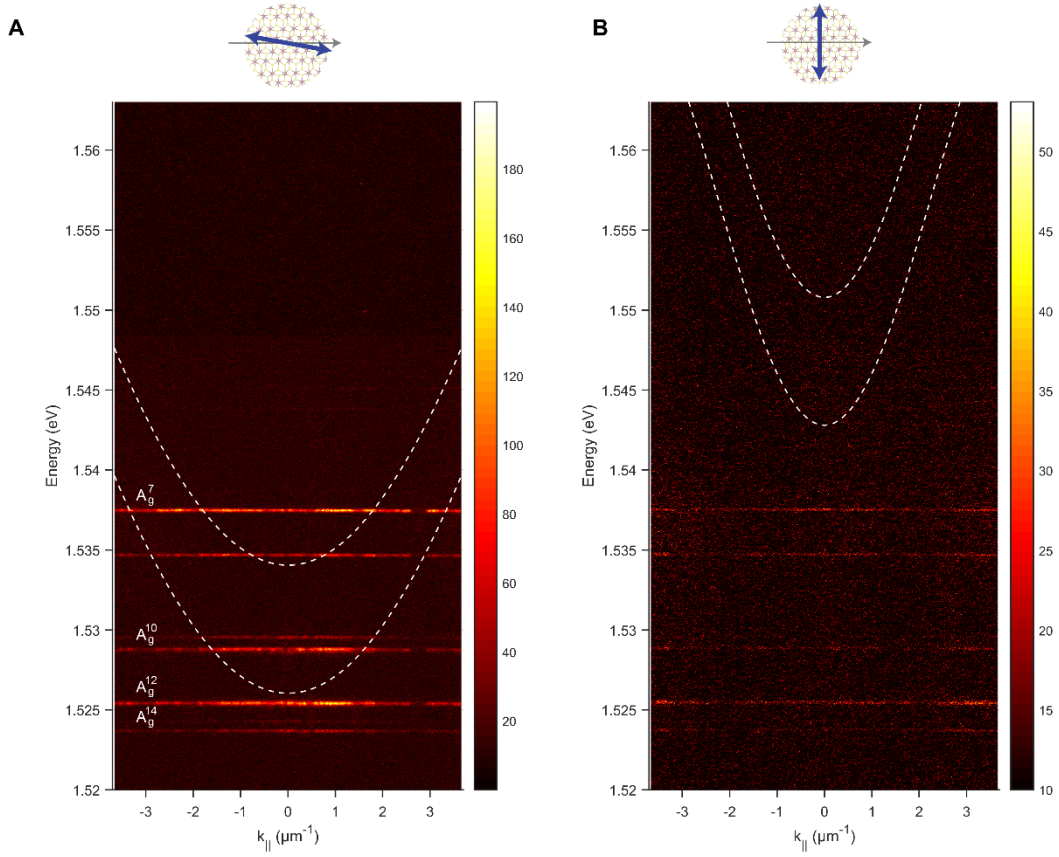


Fig. S6. Directionality of the lasing emission from the Stokes polariton modes (A) The angle-resolved Raman spectra plots display the Stokes polariton modes profiles, superimposed with the polariton band linewidth from the angle-resolved reflectance spectra (full-width half maxima indicated by dotted white lines). The figure highlights the A_g^7 , A_g^{10} , A_g^{12} and A_g^{14} modes, which exhibit lasing emission and fulfil the momentum matching condition. (B) Those same Stokes polariton modes do not lase along the d_2 axis do not display any emission pattern.

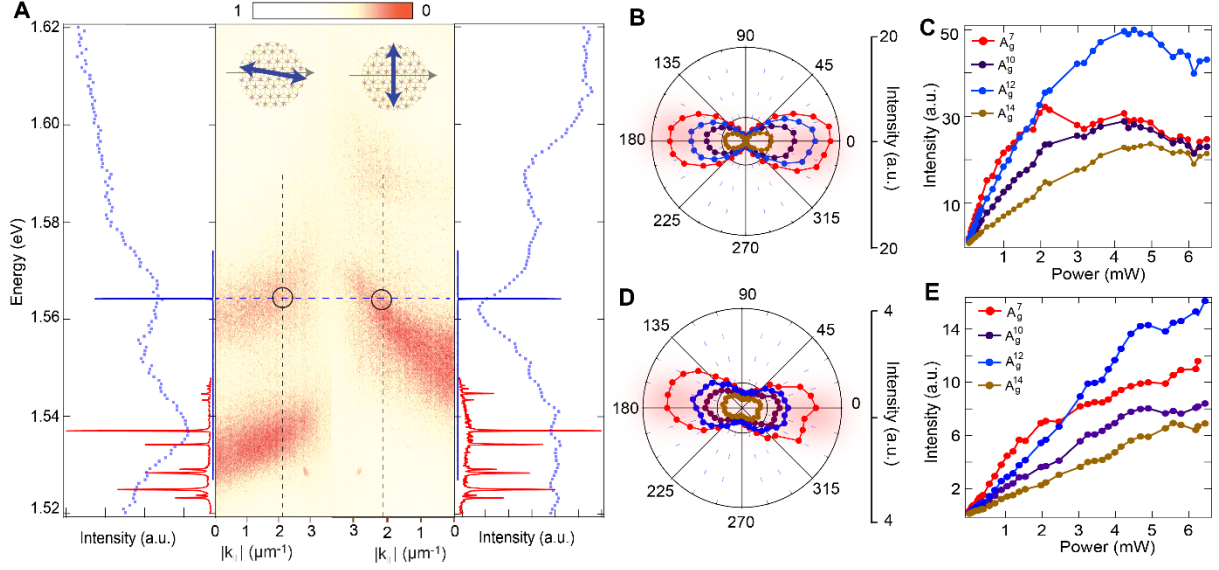


Fig. S7. Experimental results for alternative sample shown in fig. S4. (A) Angle resolved reflectance for probe beam polarization along d_1 (right) and d_2 (left) axis. EP regions in polariton dispersion for this sample are marked (black circles). Adjacent plots along the extreme left and extreme right show corresponding line profile at the EPs, and the Stokes polariton modes (red) when the pump beam (blue) is polarized along those directions. (B) Polar plot of emission intensity as a function of analyser angle for the pump beam polarization along d_1 , showing a strongly polarized emission. (C) Power dependence data for excitation along d_1 showing ZTPRL for all the Stokes polariton modes. (D) A similar polar plot as figure (B) with the pump polarization beam along d_2 . (E) The power dependence plot showing the finite threshold lasing behavior with a kink near 2 mW for A_g^{10} , A_g^{12} and A_g^{14} with pump polarization along d_2 .

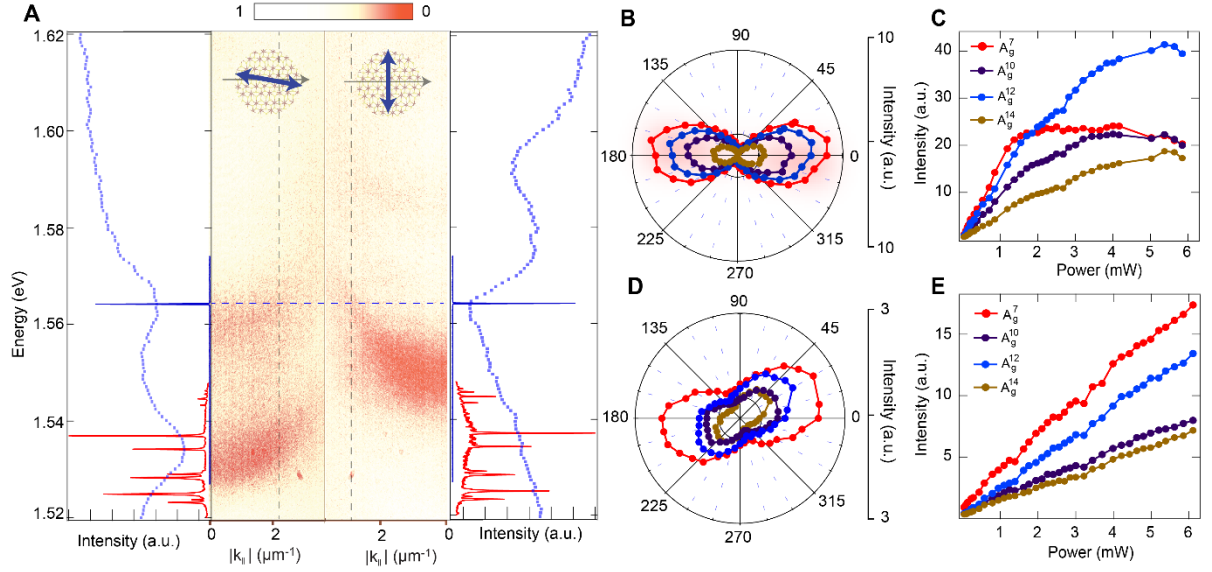


Fig. S8. Experimental results after rotating sample by 45 degrees (orientation with no EPs). (A) Angle resolved reflectance for the probe beam polarization along d_1 (right) and d_2 (left) axis. No EPs are found for this orientation. Adjacent plots along the extreme left and extreme right show corresponding line profile of the reflectivity colour plot for the in-plane momenta marked with back dashed lines, where pump beam energy coincides with the polariton branch energy. (B) Polar plot of emission intensity as a function of analyser angle for the pump beam polarization is along d_1 showing a strong polarized emission. (C) Power dependence data for excitation along d_1 showing ZTPRL for all the Stokes polariton modes. (D) A similar polar plot as figure (B) with the pump polarization beam along d_2 . Here all the modes are polarized along the different directions indicating there is no lasing happening for any mode. (E) The power dependence plot showing linear behavior of the Stokes polariton modes with no lasing threshold for pump polarization along d_2 .

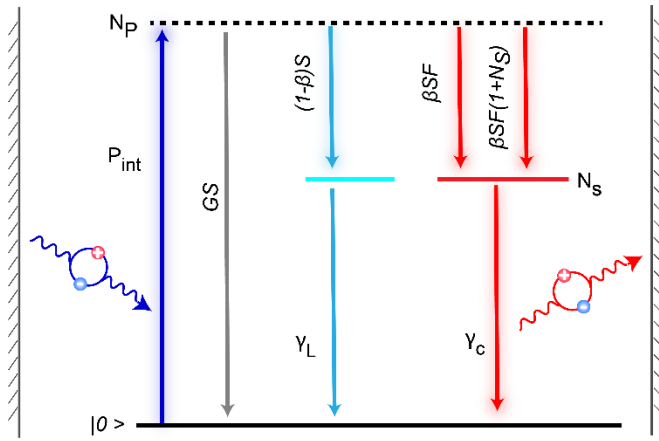


Fig. S9. Schematic showing the states and scattering terms involved in the rate equation model for stimulated resonant Raman scattering.

References:

1. Pattanayak, A. K. *et al.* A Steady-State Approach for Studying Valley Relaxation Using an Optical Vortex Beam. *Nano Lett.* **22**, 4712–4717 (2022).
2. McCreary, A. *et al.* Intricate Resonant Raman Response in Anisotropic ReS₂. *Nano Lett.* **17**, 5897–5907 (2017).
3. Zhou, Y. *et al.* Stacking-Order-Driven Optical Properties and Carrier Dynamics in ReS₂. *Adv. Mater.* **32**, 1908311 (2020).
4. Yokoyama, H. & Brorson, S. D. Rate equation analysis of microcavity lasers. *Journal of Applied Physics* **66**, 4801–4805 (1989).
5. Checoury, X., Han, Z., El Kurdi, M. & Boucaud, P. Deterministic measurement of the Purcell factor in microcavities through Raman emission. *Phys. Rev. A* **81**, 033832 (2010).
6. Bjork, G. & Yamamoto, Y. Analysis of semiconductor microcavity lasers using rate equations. *IEEE J. Quantum Electron.* **27**, 2386–2396 (1991).
7. Petrak, B., Djeu, N. & Muller, A. Purcell-enhanced Raman scattering from atmospheric gases in a high-finesse microcavity. *Phys. Rev. A* **89**, 023811 (2014).
8. Kavokin, A. V., Baumberg, J., Malpuech, G. & Laussy, F. P. *Microcavities*. (Oxford University Press, 2017).
9. Khurgin, J. B. & Noginov, M. A. How Do the Purcell Factor, the Q-Factor, and the Beta Factor Affect the Laser Threshold? *Laser & Photonics Reviews* **15**, 2000250 (2021).